The 21st-century wetting inhibits growing surface ozone in Northwestern China

Authors: Xiaodong Zhang[1,*], Yu Yan[2], Ning Zhang[2], Wenpeng Wang[3], Huabing Suo[2], Xiaohu Jian[1], Chao Wang[2], Haibo Ma[2], Hong Gao[2,*], Zhaoli Yang[2], Tao Huang[2], Jianmin Ma[1]

Affirmations:

[1] Laboratory for Earth Surface Processes, College of Urban and Environmental Sciences, Peking University, Beijing, 100871, P. R. China

[2] Key Laboratory for Environmental Pollution Prediction and Control, Gansu Province, College of Earth and Environmental Sciences, Lanzhou University, Lanzhou, 730000, P.R. China

[3] College of Atmospheric Sciences, Lanzhou University, Lanzhou, 730000, P.R. China

[*] **Corresponding author:** Xiaodong Zhang, email: zhangxd2020@pku.edu.cn; Hong Gao, email: honggao@lzu.edu.cn

ABSTRACT:

Previous studies have shown that surface air temperature (SAT) facilitates the formation of surface ozone (O_3), while relative humidity (RH) often inhibits ozone generation. However, the degree to which O_3 may respond simultaneously to rising SATs and RH due to climate change remains less understood. We conducted extensive atmospheric chemistry model scenario simulations to investigate the impacts of long-term trends of humidification and warming on summer O_3 concentrations in Northwestern China (NW) from 1998 to 2017, a period during which this region experienced both warming and the most significant wetting trend in China. We found that the summer mean O_3 level in NW increased by 19.9% during this time. The changes in meteorology led to a reduction in O_3 levels, primarily due to humidification in NW, which counteracts the warming-induced O_3 increase. We demonstrate that the wetting trend in NW will continue from 2019 to 2030 under a shared socioeconomic pathway (SSP) in conjunction with a representative concentration pathway SSP5-RCP8.5, but will either cease or shift to drier conditions from 2019 to 2060 under the SSP2-RCP4.5. No significant responses of O_3 fluctuations to RH variations were observed, partly due to manual intervention under the SSP2-RCP4.5.

Keywords: Ozone, Wetting, Warming, Northwestern China, Future projection

1. Introduction

Atmospheric humidity is recognized as a crucial factor that directly and indirectly influences the formation and evolution of surface ozone (Ghazali et al., 2022; Han et al., 2011; Kerr et al., 2020). The relationship between atmospheric humidity and surface O_3 is complex. From a chemical standpoint, humidity can modify the rates of photochemical reactions, thereby affecting O_3 formation. Additionally, humidity plays a role in generating hydroxyl radicals (OH) in the atmosphere, which are vital for breaking down volatile organic compounds (VOCs) and other pollutants (Ding et al., 2023; Ma et al., 2021). These radicals can interact with O_3 precursors, impacting the rate of O_3 production. High humidity can also enhance aerosol formation, facilitating heterogeneous reactions. Depending on the specific chemical pathways involved, some of these reactions may either generate or deplete O_3 (Eck et al., 2020). From a physical perspective, humidity is critical for cloud and fog formation as well as precipitation. The latter promotes O_3 dissolution in water droplets and its removal from the atmosphere through wet deposition, particularly during precipitation events, which weakens solar radiation and disrupts the energy balance near the surface (Ding et al., 2021; Eck et al., 2020; Kleeman, 2008; Madden and Williams, 1978; Millstein and Harley, 2009).

It has been reported that O_3 levels increased by 30% over Northern China in summer and 50% over Eastern China in autumn during a dry year compared to a wet year, indicating that wet climate conditions do not support rising O_3 levels (Ding et al., 2023). Long-term ambient O_3 measurement data indicate that rising absolute air humidity resulted in lower near-surface O_3 concentrations at temperatures of 0−30°C (Belan and Savkin, 2019). Other studies examining the relationship between O_3 concentrations and atmospheric humidity have also identified negative correlations between O_3 levels and humidity (Li et al., 2022). Nevertheless, significant knowledge gaps regarding the relationship between humidity and O_3 persist (Li et al., 2021). Most previous studies utilized short-term or instantaneous O_3 concentrations to evaluate the associations between O_3 and atmospheric humidity (Gong et al., 2021; Li et al., 2021). Their long-term relationships still require clarification. Previous investigations of the connections between climate and O_3 primarily focused on the impact of air temperature, which often overshadows the effects of other meteorological variables (Wang et al., 2024). The extent to which atmospheric humidity could significantly influence the long-term O_3 trend remains uncertain, given that the synergistic effects of warming and wetting frequently occur in a warming climate.

62   In recent decades, Northwestern China has emerged as a critical region for studying O_3

63 variability due to its unique climatic and environmental conditions. Observational studies report a

64 significant increase in summer surface O_3 concentrations across the region, with trends ranging

65 from 1.5–3.0 µg m^{-3} yr^{-1} between 2000 and 2020 (Li et al., 2020; Zhang et al., 2022). This rise has

66 been attributed to intensified anthropogenic emissions (e.g., NO_x and VOCs from energy and

67 industrial activities) and shifting meteorological patterns, including the 'warming and wetting'

68 climate regime (Yang et al., 2023). For instance, Ding et al. (2023) identified a 20% increase in

69 O_3 levels during dry years compared to wet years in arid regions, highlighting the sensitivity of O_3

70 to humidity. In this context, O_3 and RH trends in NW over the past decades likely present a unique

71 scenario to help bridge this knowledge gap. NW (Fig. S1), located in the hinterland of the Asian-

72 European continent, is Asia's largest arid and semi-arid region, characterized by limited rainfall

73 and vegetation (Koster et al., 2004; Yang et al., 2023). Meteorological records indicate that from

74 1960 to 2013, precipitation in NW increased at a rate of 0.55 mm per year (Li et al., 2012; Liu et

75 al., 2013; Yang et al., 2017). During this period, the air temperature rose at a rate of 0.034 °C per

76 year, exceeding the warming trends observed across all of China (0.025 °C per year) and globally

77 (0.013 °C per year). Although RH does not exhibit a significant growth trend during this period,

78 in the recent decade (2008-2017), it increased markedly at a slope of 0.313 in NW and 0.381 in

79 the three westernmost provinces of Xinjiang, Gansu, and Qinghai within NW. Based on these

80 records, NW appears to be entering a "warming and wetting" phase, accompanied by a rise in

81 precipitation, runoff, and lake levels (Nie et al., 2022; Peng and Zhou, 2017; Shi et al., 2002; Yao

82 et al., 2021).

83   The present study aims to address the knowledge gap in the complex and long-term

84 relationships between ozone pollution and atmospheric humidity, focusing on NW, where

85 increasing O_3 pollution, air temperature, and humidity have co-occurred (Peng and Zhou, 2017;

86 Yang et al., 2017), mainly since the early 2000s. This research provides valuable insights into the

87 broader context of air quality management and climate variability by enhancing our understanding

88 of the long-term relationship between ozone pollution and atmospheric humidity.

89

90 **2. Method and data**

91 **2.1 WRF-Chem Model Configuration**

92   Since measured O_3 concentration data in China is only available after 2013, we applied the
93   three-dimensional Weather Research and Forecasting with Chemistry (WRF-Chem) version 3.7
94   model   (http://www2.mmm.ucar.edu/wrf/users/wrf_files/wrfv3.7/updates-3.7.html)   to   predict
95   meteorology, O_3 concentrations, and other relevant data in Northwestern and mainland China. The
96   model domain spans the entire mainland China at a $20\,km \times 20\,km$ resolution, extending vertically
97   from the surface to the lower stratospheric ozone layer at an altitude of 50 hPa with 30 staggered
98   vertical layers. This vertical segmentation facilitates a deepened comprehension of the O_3
99   dynamics within the region, enabling the capture of its detailed behavior throughout the
100   atmospheric stratifications (Li et al., 2020; Zhang et al., 2020, 2022). Detailed physical and
101   chemical schemes contributing to O_3 formation in WRF-Chem and emission input followed
102   previous studies (Bei et al., 2018; Bossioli et al., 2016; Liao et al., 2015; Tie et al., 2009; Wild et
103   al., 2000) and are presented in Section S1 in the Supplement and Tables S1-S2. The soil NO, NO_x,
104   and HONO emissions have been considered a necessary process contributing to surface ozone
105   formation in recent years (Lu et al., 2021). However, given the lack of soil emission inventories
106   of these reactive nitrogen species in China and the world, the present modeling study did not take
107   these processes into consideration. The aerosol feedback mechanisms include the direct and
108   indirect effects, the both are considered in WRF-Chem. The model simulations with a nudging
109   option in WRF were conducted from June 1st to August 31st in each summer from 1998 to 2017,
110   with a time-step of 30s. A spin-up time of three days was adopted before June 1st in each summer.
111   Further details are referred to Section S1 in the Supplement.

112   Located in the upstream of China in terms of dominant prevailing westerly winds in the mid-
113   latitudes of the Northern Hemisphere, it is expected that Northwestern China would receive more
114   O_3 and its precursors from foreign sources in Eurasian countries to the west of China compared to
115   Eastern China (Li et al., 2014; Li et al., 2016). Such "upstream" effect is implicitly accounted for
116   in meteorology and chemistry lateral boundary conditions under an open boundary approach
117   (https://www2.acom.ucar.edu/wrf-chem). These boundary conditions typically come from global
118   chemical transport model outputs (e.g., GEOS-Chem, MOZART) that themselves simulate O_3 on
119   a global scale (including those upstream regions), chemical reactions, wet and dry deposition, and
120   atmospheric transport processes. These datasets are usually generated or assimilated from global
121   models and observations. The lateral boundary conditions govern the fluxes and concentration
122   levels of pollutants entering the model domain from external (upstream) regions. They represent

123   the environmental or regional background concentration outside the model domain, which already

124   integrates emissions and transport influences from a broader region (including upstream areas).

125   The lateral boundary conditions of chemical species in our modeling exercise were estimated from

126   MOZART-4 reanalysis driven fields (Emmons et al., 2010; Zhang et al., 2020) on a daily basis.

127   The ERA-Interim data with a 6-hourly time resolution and $0.7° \times 0.7°$ lat/lon spatial resolution

128   provided by the ECMWF (European Centre for Medium-Range Weather Forecasts) were adopted

129   as lateral boundary conditions of meteorology. Further, since the multiple model scenario

130   simulations in our study used the same lateral boundary conditions, this effectively removed the

131   influences of precursor emissions and atmospheric transport from Eurasian countries but focused

132   on the wetting impact on O_3 evolution in the internal model domain (China).

2.2 Trend

134   ~~Considering relatively short data time series (1998-2017), the~~The Mann-Kendall (MK) Test and

135   Sen's slope (El-Shaarawi and Niculescu, 1992; Kendall, 1949; Mann, 1945) were used to examine

136   the trend of O_3, near-surface air temperature (SAT) at the 2m height, and relative humidity (RH, %)

137   at the 2m height. The Mann-Kendall (MK) Test and Sen's Slope are both non-parametric statistical

138   methods commonly used for analyzing trends in time series data. The MK Test helps determine if

139   there is a significant trend, and Sen's slope quantifies the strength and direction of the trend (slope

140   value).

141   Interannual ozone variability in Northwestern China is primarily driven by large-scale

142   meteorological shifts (e.g., warming, humidification) and regional precursor emissions, rather than

143   diurnal processes. Previous studies (Cooper et al., 2014; Li et al., 2020) have revealed that long-

144   term O_3 trends (interannual and interdecadal scales) are robustly represented by seasonal or annual

145   mean concentrations, as diurnal variations associated with daytime photochemistry and nighttime

146   titration are statistically insignificant. For example, Ding et al. (2023) reported that separating

147   daytime and nighttime O_3 yielded negligible differences (>95% correlation) in O_3 trend over a 20-

148   year period in arid seasons in China.

2.3 O₃ Attribution to Meteorology and Emission

150 We calculated the fraction (percentage change, %) to account for O_3 attribution to meteorology
151 and emission subject to different model scenarios. For example, we define the fraction

152 $F_{O3} = (C_{S3} - C_{S1}) / C_{S1} \times 100\%,$ (1)

153 as the attribution of O_3 concentration to emissions, where C_{S1} and C_{S3} are the summer surface O_3
154 air concentrations from the base (S1) and fixed meteorology (S3) scenarios.

155 **2.4 Data**

156 To initialize and prescribe boundary conditions in the WRF model from 1998 to 2017,
157 meteorological data were sourced from the ERA-Interim reanalysis from the European Centre for
158 Medium-Range Weather Forecast (ECMWF,
159 ~~https://www.ecmwf.int/en/forecasts/datasets/reanalysisdatasets/era-~~
160 ~~interim).~~https://www.ecmwf.int/en/forecasts/datasets/reanalysisdatasets/era-interim). This allows
161 the adoption of the open boundary conditions to dynamically account for cross-regional O_3 and
162 precursor transport, and to resolve both local photochemical production and contributions from
163 transboundary sources, ensuring a comprehensive representation of O_3 dynamics.
164 Anthropogenic emissions were collected from the Emissions Database for Global
165 Atmospheric Research (EDGAR) version 4.3 on a spatial resolution of $0.1° \times 0.1°$, which was
166 available when we started this modeling investigation. A grid-mapping program implemented the
167 emissions into the WRF-Chem (Crippa et al., 2018; Mo et al., 2017). Biogenic emissions were
168 simulated using MEGAN version 2.1 (Guenther et al., 2006, 2012). A recent study suggests that
169 temperature can alter precursor emissions (Pfannerstill et al., 2024). However, since available
170 emission inventories worldwide, including the widely-used EDGAR inventory, did not account
171 for the influence of meteorology, typically the air temperature, on emissions but only considers
172 emissions from anthropogenic and natural sources, the emissions input in the present modeling
173 might be subject to additional uncertainties. The reduction of these uncertainties will depend on
174 improved inventories that take the meteorological effect into account.
175 We have replaced WRF land-use change (LUC) data with Chinese land use/land cover remote
176 sensing monitoring database provided by the Data Center for Resources and Environmental
177 Sciences, Chinese Academy of Sciences (RESDC) (http://www.resdc.cn), which significantly
178 improved China's LUC in our investigation of the effect of urbanization on O_3 pollution in China

179 (Zhang et al., 2022). The new LUC data has a spatial resolution of 1 km × 1 km, which is
180 extrapolated to the WRF-Chem grid cells (20 km × 20 km).

181   Considering that the warming and wetting trends in NW might persist in the coming decades,
182 we also projected future O_3 and meteorology in 2019, 2030, and 2060 in the WRF-Chem model
183 framework and simulations, respectively. We collected future anthropogenic emission data from
184 the Dynamic Projection Model for Emissions in China (DPEC Inventory – MEICModel,
185 http://meicmodel.org.cn), with a spatial resolution of 0.25° × 0.25° longitude and latitude (Cheng
186 et al., 2021, 2023; Tong et al., 2020). The meteorological data was collected from Shared
187 Socioeconomic Pathways (SSP) and Representative Concentration Pathways (RCP) climate
188 scenarios under the CMIP6 framework (https://aims2.llnl.gov/search/cmip6/), with the MPI-
189 ESM1-2-HR model (Eyring et al., 2016). Compared with other models, MPI-ESM1-2-HR has
190 higher resolution and can simulate the complex interactions within the climate system, including
191 all climate scenarios (SSP2-RCP4.5 and SSP5-RCP8.5) targeted by this study, and has been widely
192 used in WRF simulations.

193 **2.5 Model Evaluations**

194   Rigorous comparisons between simulated O_3 concentrations and measured data were
195 conducted and presented in Figs. S2-S7 and Section S2 in the Supplement. Overall, the simulated
196 O_3 concentrations agree reasonably well with measured data, demonstrating a high level of
197 reliability of modeling results.

198 **2.6 Model Scenario Setup**

199 We established several model scenarios to distill signals of meteorological conditions, primarily
200 SAT and RH, in modeled O_3 concentrations. Detailed configurations are provided in Table 1. The
201 first scenario (S1) serves as the baseline, incorporating summer-specific meteorological variables
202 and emissions from 1998 to 2017 into WRF-Chem simulations, and is thus considered a realistic
203 scenario. In the second scenario (S2), we fixed emissions from 1998 throughout the period from
204 1998 to 2017, aiming to assess the significance of the meteorological effect on O_3 variation. In the
205 third scenario (S3), we fixed meteorology from 1998 during the same period, thereby emphasizing
206 the importance of emissions in O_3 variation. To evaluate the sensitivity of scenario S3, we also
207 conducted an additional WRF-Chem run by fixing SAT and RH only in 1998 (scenario S4) and

208   compared the modeled O_3 concentrations with those simulated in scenario S3 for 2004. ~~The results~~

209   ~~indicate minor differences between model scenario S3 and the results from the fixed SAT and RH~~

210   ~~model run (Fig. S8).~~Overall, we found minor differences (two tails T-test = 0.1065) between model

211   scenario S3 and the results from the fixed SAT and RH model run (Fig. S8) but slightly stronger

212   O_3 pollutions subject to fixed RH and SAT scenario than S3 results can be discerned in the

213   Northern China Plain. ozone concentrations under fixed SAT and RH in 1998 seemed higher than

214   fixed all meteorology in 1998 (S3 scenario). We further calculated the differences of the planetary

215   boundary layer heights (PBLH) between the two scenarios (fixed RH and SAT scenario minus

216   scenario S3). The results are illustrated in Fig. S9. Negative PBLH differences can be seen in many

217   areas across China, including the NCP, indicating that fixed SAT and RH scenario reduced PBLH,

218   which often associates with stronger air pollution within the PBLH. By calculating the differences

219   and fractions, we can discern the contributions of meteorology and emissions to O_3 formation and

220   destruction. We also established two additional model scenarios to project the responses of O_3

221   concentrations to future meteorology and emissions in NW based on CMIP6 pathways SSP2-

222   RCP4.5 and SSP5-RCP8.5, specifically for 2019, 2030, and 2060, respectively. Detailed

223   descriptions of these two pathways and the corresponding data are presented in Section S3 in the

224   Supplement.

225

226

227

228

229   **Table 1.** Model scenarios.

Scenario	Simulation period	Meteorology	Emission	LUC
S1	1998-2017	Varied	Varied	Varied
S2	1998-2017	Varied	Fixed (1998)	Varied
S3	1998-2017	Fixed (1998)	Varied	Varied
S4	2004	Only fixed SAT and RH (1998)	Varied	Varied
S5	1998-2017	Varied	Varied	Fixed (1998)

SSP2-4.5	2019, 2030, 2060	Varied	Varied	Varied
SSP5-8.5	2019, 2030, 2060	Varied	Varied	Varied

230

3. Results and Discussion

3.1 Summer Ozone Trends

Figures 1a and 1b present MK-Test statistics and Sen's slope estimated temporal trends of summer O_3 concentrations from 1998 to 2017 under scenario S1 (base scenario) and S3 with fixed meteorology in China. In the S1 scenario (Fig. 1a), O_3 concentrations exhibit statistically significant declining trends in the northernmost regions, spanning from Northeastern Xinjiang to Northeastern China, with the most significant decline occurring in Inner Mongolia. Increasing O_3 concentrations are observed along Tianshan Mountain in Xinjiang, western Tibet, and central China. The fixed meteorology scenario (S3, Fig. 1b) shows a monotonically increasing trend across China, indicating continuously rising O_3 levels for the past two decades due to growing precursor emissions, except for some grid cells in the Yangtze River Delta (YRD), the Pearl River Delta (PRD), the Beijing-Tianjin metropolitan area, and other sporadic regions, where MK-Test and Sen's slope identified statistically significant negative O_3 trends. Previous studies have also noted the negative trends over the past decade in these regions (Hu et al., 2024; Li et al., 2022; Wang et al., 2020; Yu et al., 2021). The Beijing-Tianjin area, YRD, and PRD are three critical regions under China's joint efforts to prevent and control air pollution. Regional emission mitigation in these areas may lead to varying reductions in precursor emissions and declines in O_3 concentrations. Overall, increasing precursor emissions have dominated the O_3 trend in China, as meteorology remained constant during this period. This is evidenced by the linear trends of NO_x and NMVOC (Non-methane VOC) emissions in China from 1998 to 2017 (Fig. S9S10). When comparing the MK-Test and Sen's slope results between the two scenarios model runs, (Fig. 1c), the meteorological conditions from 1998 to 2017 overshadowed the effects of emissions, primarily contributing to the declining O_3 levels (negative trends) in the northernmost regions of China, extending from Inner Mongolia to Northeastern China. Our modeling result shows that mean summer O_3 concentration averaged over Inner Mongolia reached the maximum in 2007 and

256 slightly declined thereafter (Fig. ~~S10~~S11). This can be partly attributed to relatively lower
257 precursor emissions resulting from the sparse population and limited industrial activities in this
258 part of China, though having a growing trend (Zhang et al., 2022, 2023).

259
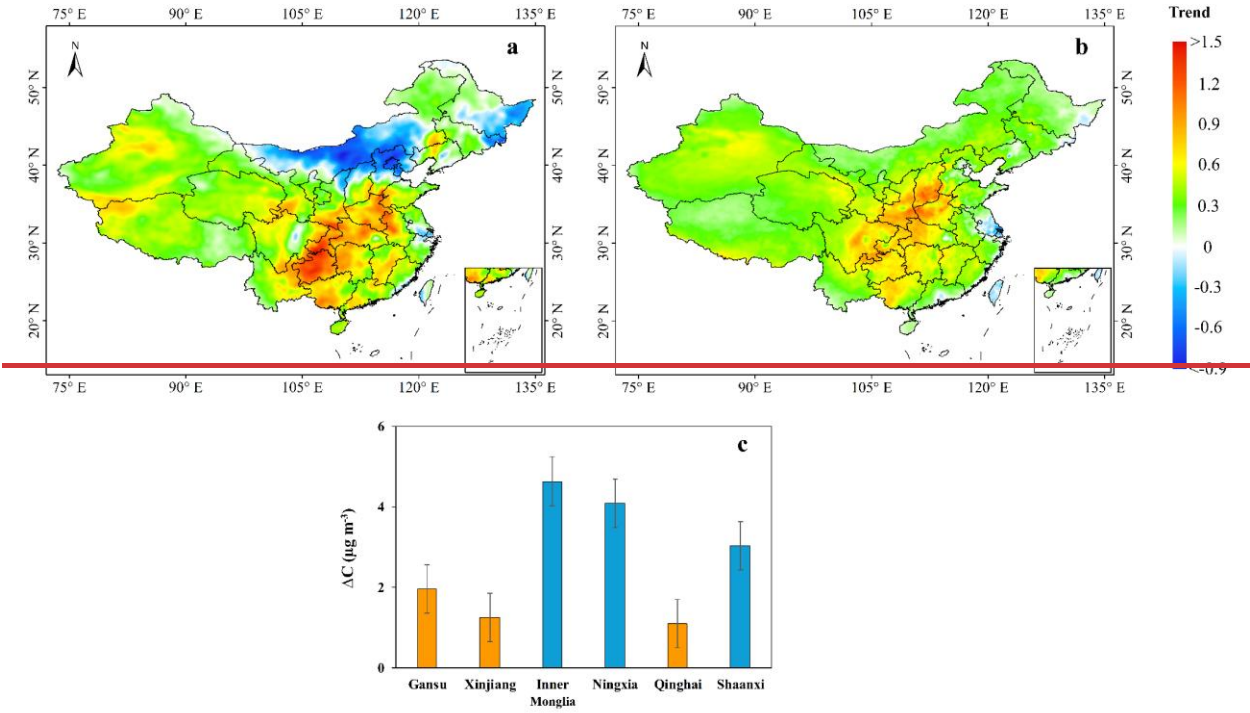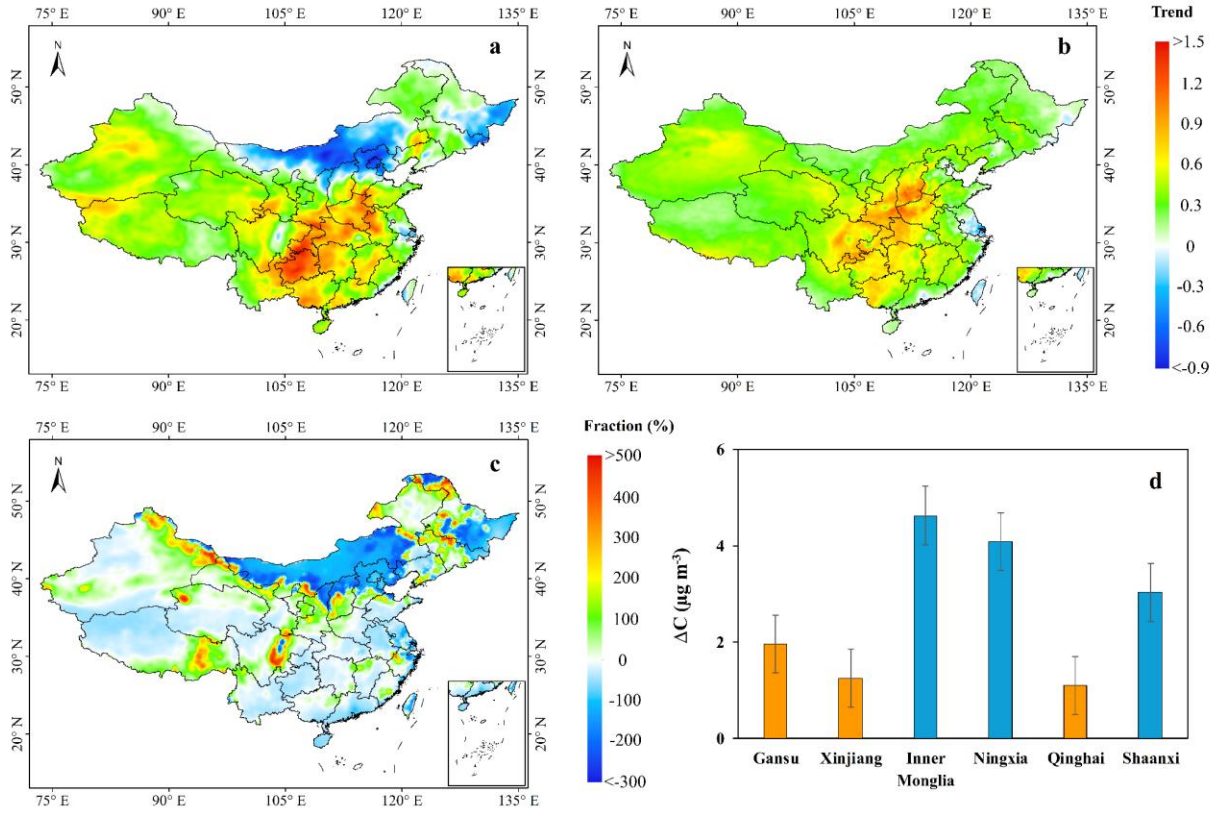
Figure 1. MK-Test and Sen's slope estimated summer O_3 concentration trend and O_3 attribution (fraction or percentage change, %) under baseline (S1) and fixed meteorology (S3) scenarios from 1998 to 2017, respectively. (a) MK-Test and Sen's slope estimated trend from the base scenario S1, the trends of concentrations are well within the MK-Test statistically significant range at 95% confidence level in terms of |Z|>1.96 criteria; (b) same as Fig. 1a but for fixed meteorology scenario S3; (c) fraction of O_3 concentration trend between the model scenarios 1 and 3 from 1998 to 2017; (d) mean differences of summer mean O_3 concentrations averaged from 1998 to 2017 between the model scenarios 1 and 3, defined by $\overline{\Delta O_3} = \bar{O}_{3,S1} - \bar{O}_{3,S3}$, where $\bar{O}_{3,S1}$ and $\bar{O}_{3,S3}$ stand for mean summer O_3 concentrations averaged over 1998 to 2017, respectively. $\overline{\Delta O_3}$ in three Westernmost provinces of NW is shown by yellow bars and blue bars for three Easternmost provinces of NW. Error bar in Fig. ~~1c~~1d stands for ±1 STD.

To discern potential influences of meteorology on O_3 concentrations at the provincial level, we estimated the differences of summer mean O_3 concentrations averaged from 1998 to 2017 between model scenarios 1 (S1) and 3 (S3), defined by $\overline{\Delta O_3} = \bar{O}_{3,S1} - \bar{O}_{3,S3}$. Figure ~~1c~~1d illustrates $\overline{\Delta O_3}$ in each province of Northwestern China. Since the mean O_3 levels under scenario S1 were greater than those under scenario S3 with fixed meteorology in 1998, although in some years we also identified negative ΔO_3 in the three westernmost provinces (Xinjiang, Gansu, and Qinghai), we would expect positive $\overline{\Delta O_3}$, as shown in Fig. ~~1c~~1d. In this context, the values of $\overline{\Delta O_3}$

278   indicate the extent of meteorological influence on O_3 concentrations. Specifically, the smaller $\overline{\Delta O_3}$,

279   the stronger meteorological influences, as a smaller $\overline{\Delta O_3}$ suggests that O_3 levels with varying

280   meteorology (S1) are closer to those with fixed meteorology in 1998 (S3). We highlighted the

281   three provinces with smaller $\overline{\Delta O_3}$ (<2 μg m^{-3}) using yellow bars, all located in Westernmost NW,

282   indicating a weaker increase in O_3 concentrations in these three westernmost provinces compared

283   to others, aligning well with the RH trends in these provinces, as compared to the other three

284   provinces located in the east of NW (Inner Mongolia, Ningxia, and Shaanxi), as mentioned in the

285   Introduction. As shown in Fig. ~~S11~~S12, modeled concentration fractions under the S2 model

286   scenario with fixed emissions in 1998 in the three westernmost provinces of NW are negative,

287   indicating that meteorology tended to inhibit the increase in summer ozone concentrations,

288   particularly in Xinjiang, Gansu, and Qinghai, confirming the result in Fig. ~~1c~~1d. In the other three

289   provinces to the east of NW, we observe larger $\overline{\Delta O_3}$ values, suggesting that meteorology, along

290   with precursor emissions, tended to enhance O_3 levels from 1998 to 2017. Consequently, we would

291   expect that meteorology favored O_3 growth in these three eastern provinces of NW.

292   **3.2 Associations of summer ozone with wetting and warming**

293
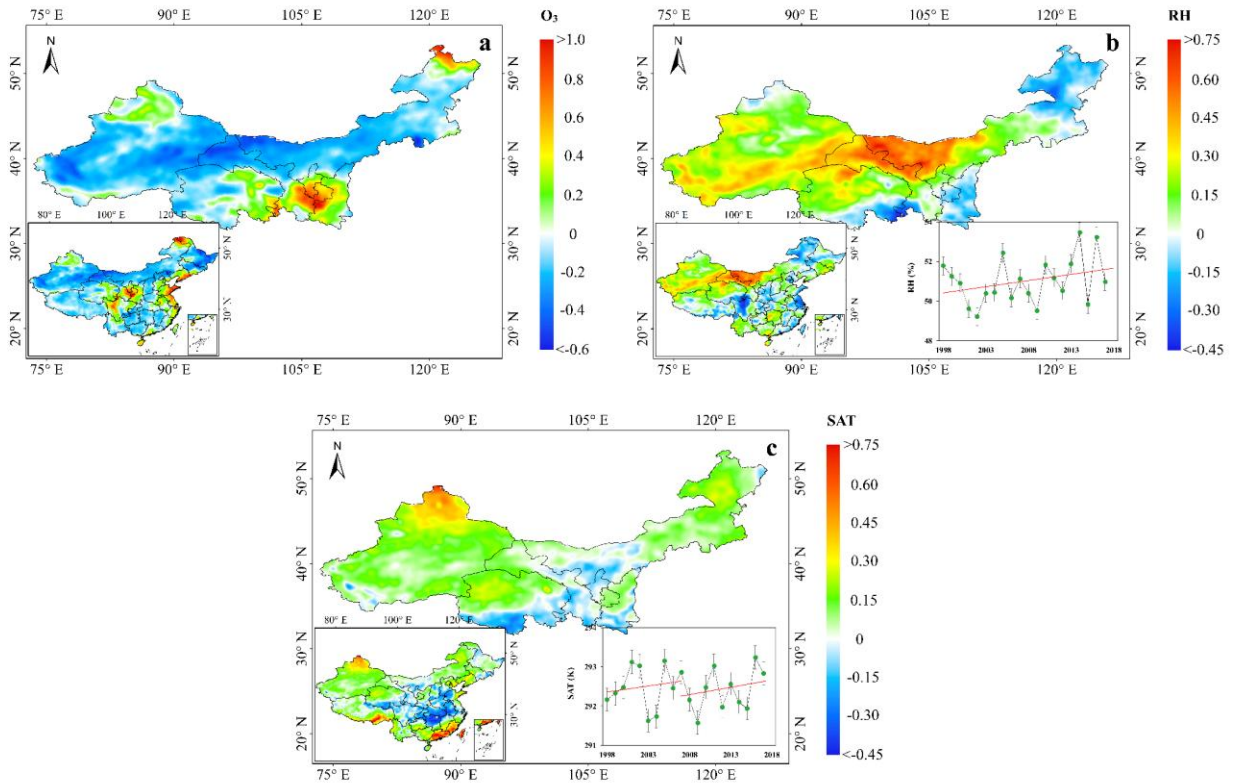
Figure 2. (a) MK-Test statistics for the trends of summer O_3 concentrations from 1998 to 2017 subject to model scenario 2 (S2) with fixed emissions in 1998, (b) MK-Test statistics for summer RH from 1998 to 2017, the line chart on the low-right corner illustrates summer RH in NW from 1998 to 2017 under scenario 2, (c) MK-Test statistics for trend of summer SATs from 1998 to 2017, the line chart shows summer SATs averaged over Northwest China from 1998 to 2017, under scenario 2. Contour figures on the low left corner of Figs. 2a-2c illustrates MK-Test statistics for O_3 trends under fixed emission (model scenario 2) and modeled RH and SAT trends in mainland China from 1998 to 2017. The trends are well within the statistically significant range at 95% confidence level in terms of |Z|>1.96 criteria.

Figure 2a illustrates the MK-Test statistics of gridded summer O_3 concentrations from 1998 to 2017 subject to the model scenario S2 with fixed emissions and annually varied meteorology, aiming to highlight the effect of meteorology on O_3 evolution. A notable decline in summer O_3 ozone concentrations is evident in most areas of mainland China, except for the Northern China Plain, central China, the Sichuan Basin, and the Guanzhong Plain (inner figure on the left-low corner of Fig. 2a). The declining O_3 trends are also evident in most regions across NW with the most substantial decrease occurring in west Gansu, northwest Inner Mongolia, and Xinjiang. With fixed emission, such an O_3 falling trend is induced primarily by meteorology (climate). Considering that air temperature and humidity are two key meteorological factors influencing O_3 fluctuations, we present the MK-Test statistics of the trends of summer relative humidity (RH, %) at the 2 m height in Northwestern and mainland China (illustrated in the lower-left corner of Fig. 2b), along with their annual variations depicted in a line chart in the lower-right corner of Fig. 2b. We also present the surface air temperature (SAT, K) in Northwestern and mainland China in a line chart in the lower-right corner of Fig. 2c. Compared to many places across Eastern and Central China where RH has negative or drying trends (left-low corner of Fig. 2b), RH in NW showed a marked surge, suggesting pronounced wetting, as reported before (Peng and Zhou, 2017). This can also be seen in the annual changes in the mean RH averaged over NW (the line chart on the right-low corner of Fig. 2b) from 1998 to 2017, dominated by an overall upward RH trend with a mean growth rate of 1.9% per year. Likewise, NW also experienced warming during the same period, as shown in Fig. 2c, particularly in the western part of NW, including Xinjiang, western Gansu Province, and Qinghai Province. NW has been undergoing one of the most significant warming trends in the nation. Between 2005 and 2017, NW, particularly the Xinjiang region, has warmed by over 0.5 K with a rate of 0.04 K/yr. In contrast, eastern and Central China show a cooling trend. The rising SAT trend and falling O_3 trend are in contrast to the common knowledge that increasing

326 SATs should enhance O_3 levels. The result thus implies that SATs did not dominate the O_3 trend

327 in NW.

328

329
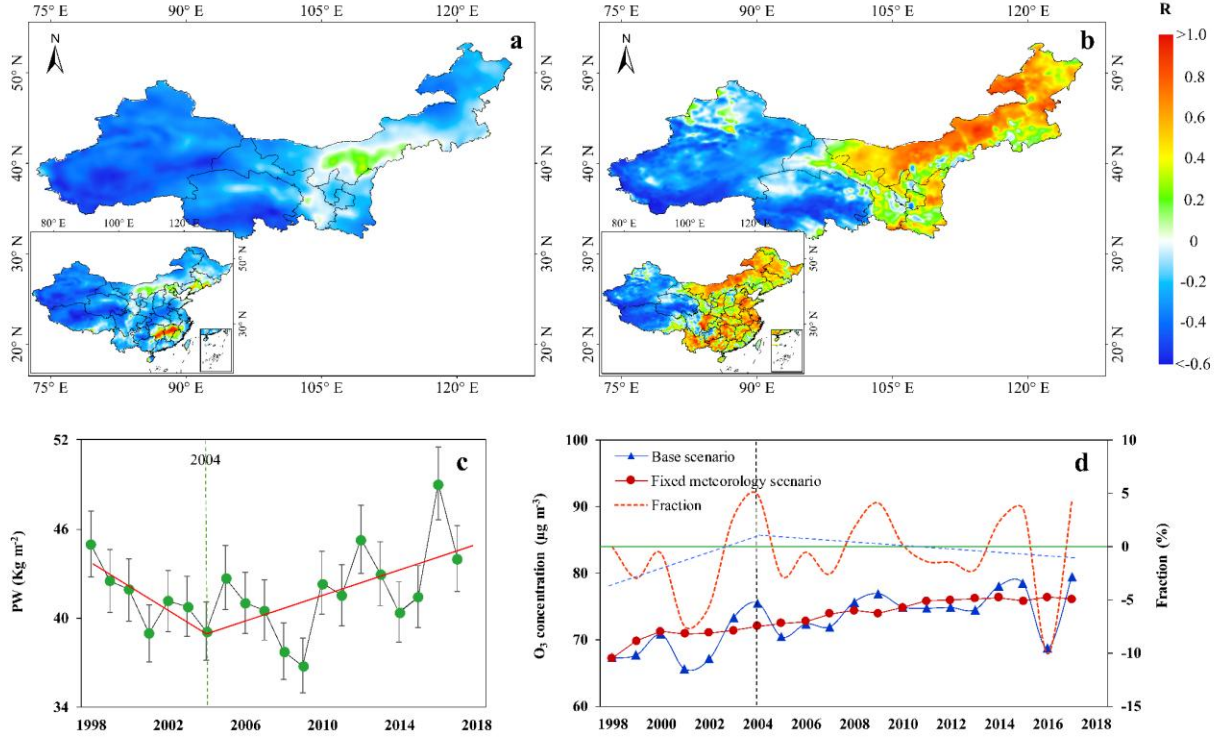
330 **Figure 3.** (a) Pearson correlation (R) between summer O_3 concentration and RH from 1998 to 2017 under S2
331 scenario, (b) R between summer OH radical concentration and O_3 concentration from 1998 to 2017 under S2
332 scenario, (c) summer surface precipitable water (PW) in the bounded area of NW from 1998 to 2017, error bar
333 stands for ±1 STD and red solid line stands for linear trend, (d) summer O_3 concentrations under Scenarios 1
334 (dark blue solid line with triangles) and 3 (red solid line with circles) scaled on the left-Y axis, and their fractions
335 $F_{O3} = (C_{S1} - C_{S3}) / C_{S3} \times 100\%$ (red dashed line) in three Westernmost provinces of HW (Xinjiang, Qinghai,
336 and Gansu), where C_{S1} and C_{S3} are the summer (June to August) surface O_3 air concentrations from the base (S1)
337 and fixed meteorology (S3) scenarios, scaled on the right-Y axis, the blue dashed line in Fig. 3d is a linear fitting
338 line from 1998 to 2004 and 2004 to 2017, respectively. The green solid line represents the zero-value line of the
339 fraction.

340   As mentioned earlier, since rising temperatures favor O_3 formation while increasing humidity

341 is detrimental to O_3 growth, it is intriguing to investigate which of these two meteorological factors

342 contributes more to the O_3 trend in NW. We first calculated linear correlation coefficients between

343 RH and O_3 concentrations modeled from the S2 scenario (fixed emissions) from 1998 to 2017

344 across Northwestern and mainland China (bottom left corner of Fig. 3a). Strong negative

345 correlations are evident in most regions of Xinjiang, Qinghai, and Western Gansu. These negative
346 correlations indicate declining O_3 concentrations with rising RH. To highlight the influences of
347 RH and precipitation on summer O_3 variation, Fig. 3d illustrates modeled mean summer O_3
348 concentrations averaged over three Westernmost provinces of HW (Xinjiang, Qinghai, and Gansu)
349 under the base scenario S1 with annually varying summer meteorology and emissions, and S3 with
350 fixed meteorology in 1998 and annually varying emissions averaged over NW, along with the
351 concentration fractions (%, red dashed line) between the two scenarios from 1998 to 2017. O_3
352 concentrations exhibit the same increasing trend primarily driven by rising precursor emissions.
353 However, the S1 scenario shows more significant annual fluctuations (solid dark blue line in Fig.
354 3d) compared to the S3 scenario (solid red line in Fig. 3d). These stronger fluctuations can be
355 attributed to the influence of meteorology. Since scenarios 1 and 3 shared the same emissions and
356 chemistry, the concentration fractions quantify the contributions of meteorology to the O_3 trend
357 alone. As shown, the fractions increased from 1998 to 2004, decreased thereafter, and turned
358 negative since 2009 (the red dashed lines), indicating that meteorology has led to declining O_3
359 concentrations since 2005 in NW. Among the two key meteorological factors influencing O_3
360 formation, increasing SAT (Fig. 2c) tends to elevate O_3 levels, which contradicts the decreasing
361 and negative O_3 fractions. Consequently, RH likely plays a more significant role in the O_3 trend in
362 NW, as rising RH aligns well with the decreasing and negative O_3 fractions.

363 Figure 3c displays the mean summer surface precipitable water (PW, kg/m2) over the region
364 bounded between 75 – 100°E in Northwest China from 1998 to 2017, collected from the NCAR
365 reanalysis (https://psl.noaa.gov/cgi-bin/data/composites/printpage.pl). One can identify a slow
366 decrease in PW from 1998 to 2004 and a rapidly growing PW thereafter. Since warming
367 exacerbates drought in arid and sub-arid NW (Lian et al., 2021), growing precipitation in NW
368 implies that increasing humidity might play a more significant role than warming in the changing
369 climate, which acts to reduce O_3 levels via precipitation washout and chemistry. A close look at
370 Figs. 2b, 2c, and Fig. 3a indicate that more substantial warming and wetting occurred in Xinjiang,
371 Gansu (including westernmost of Inner Mongolia), and Qinghai provinces. We compared the
372 fractions of provincial mean summer RH and summer O_3 concentrations from the fixed emissions
373 and annually varying meteorology scenario (S2) between 1998 and 2017 (Fig. 4a), defined by $f =$
374 $(Y_{2017} - Y_{1998}) / Y_{1998} \times 100\%$, where f is the concentration or RH fractions and Y_{1998} and Y_{2017} stand
375 for O_3 concentrations or RH in 1998 and 2017, respectively, thereby to highlight the net effect

376   from meteorology. The most significant fraction of O_3 concentration was identified in Inner
377   Mongolia at 9.9%, followed by Ningxia (5.7%), Shaanxi (5.5%), Gansu (2.8%), Xinjiang (1.6%),
378   and Qinghai (-1.5%), respectively. Among the six provinces, Xinjiang and Gansu accounted for
379   smaller O_3 fractions, and Qinghai accounted for a negative fraction (Fig. 4a), indicating that O_3
380   levels in these three provinces inclined less significantly or even declined (Qinghai) between 1998
381   and 2017 than the other three provinces. Interestingly, more significant O_3 fractions, meaning
382   growing O_3 levels for the two decades in Inner Mongolia, Ningxia, and Shaanxi, correspond to
383   smaller (Ningxia) or negative (Inner Mongolia and Shaanxi) RH fractions, meaning falling RH. In
384   contrast, more diminutive and negative O_3 fractions in Xinjiang, Gansu, and Qinghai provinces
385   are associated well with the stronger increasing trend of summer RH by MK-test (Figs. 2b and 4a)
386   at the growing rate of 9.8% in Xinjiang, 8.9% in Gansu, and 9.9% in Qinghai from 1998 to 2017,
387   respectively. While the weak or falling summer O_3 levels in three provinces respond to both
388   growing RH and SAT trends (Fig. 2b and 2c), since growing SATs tend to enhance O_3
389   concentrations but modeled O_3 respond weakly to rising SAT in these three provinces, the result
390   demonstrates again that the wetting might inhibit O_3 formation and increment for the past decades
391   in NW.
392
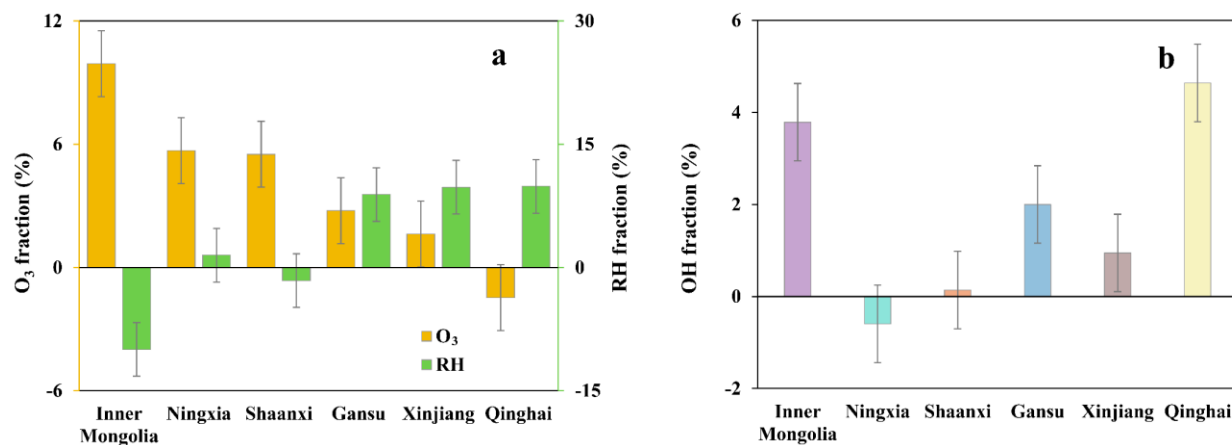
394   **Figure 4.** Summer RH, O_3, and OH radical fractions between 1998 and 2017 in six provinces of NW under the
395   fixed emission scenario (S2). (a) RH and O_3 fractions, O_3 fractions are scaled on the left Y-axis, and RH fractions
396   are scaled on the right Y-axis, (b) OH radical fractions. Error bars denote ±1 STD.

397   It is worthwhile to point out that model scenario 2 with fixed emissions also considers
398   chemistry, in which OH radicals and water vapor can interact. The primary source of OH radicals

399   in the atmosphere is the reaction between water vapor (H_2O) and excited oxygen atoms ($O(^1D)$),

400   which are formed by the photolysis of ozone (O_3) by ultraviolet (UV) radiation. The OH radicals

401   react with ozone to form oxygen (O_2) and the excited oxygen atom $O(^1D)$, which can further react

402   with water vapor to regenerate two OH radicals:

403        $O_3 + OH \rightarrow O_2 + O(^1D)$,

404        $O(^1D) + H_2O \rightarrow 2\ OH.$ (2)
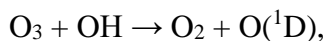
405   This reaction does not lead to a net reduction in OH radicals but contributes to ozone removal by

406   initiating reactions that lead to the formation of less reactive species. Figure 3b is a correlation

407   diagram between modeled summer O_3 concentrations and OH radicals in NW and mainland China

408   (the left-low corner of Fig. 3b) subject to the fixed emission scenario (S2). The spatial pattern of

409   correlation coefficients in NW is, to some extent, similar to that between O_3 concentrations and

410   RH (Fig. 3a), showing the negative associations between OH radicals and O_3 concentrations,

411   particularly in Xinjiang and Qinghai with the most significant wetting trend, suggesting that

412   increasing OH radicals reduce O_3 levels. Figure 4b displays the fractions of provincial mean

413   summer OH radicals from the fixed emissions and annually varying meteorology scenario (S2)

414   between 1998 and 2017. Relatively larger positive fractions can be discerned in Xinjiang, Qinghai,

415   and Gansu, meaning increasing OH radicals in these provinces as a result of increasing RH (Eq.

416   1), which corresponds to higher RH fractions and lower O_3 fractions. An exception occurs in Inner

417   Mongolia, where the large positive OH radical fraction (Fig. 4b) is associated with negative RH

418   and large O_3 fractions (Fig. 4a). OH radicals show an increasing trend (Fig. ~~S12~~S13) which agrees

419   with the positive correlation between OH and O_3 concentrations shown in Fig. 3b. This puzzling

420   from the modeling results needs further investigations.

421   There are several primary mechanisms of OH radicals leading to O_3 reduction, including the

422   reaction with VOCs to form peroxyl radicals (RO_2), the reaction of RO_2 with nitrogen oxides (NO_x

423    $= NO + NO_2$) to form nitrogen dioxide (NO_2) and other compounds, and photodissociation of NO_2.

424   Figures ~~S9a~~S10a and ~~S9b~~S10b show the MK test estimated NO_x and NMVOC emission trends

425   from 1998 to 2017. While increasing NO_x is observed in NW (Fig. ~~S9a~~S10a), its emission levels

426   are considerably lower than in Eastern and Southern China (Fig. ~~S9c~~S10c). Both NMVOC

427   emission levels and trends in NW are significantly smaller than in Eastern and Southern China due

428 to lower populations and less developed economies (Fig. ~~S9b~~S10b and ~~S9d~~S10d). Hence, it is

429 likely that the reaction of water vapor (H_2O) with excited oxygen atoms ($O(^1D)$) produced by the

430 photodissociation of ozone by UV light plays a specific role in the negative correlation between

431 O_3 and OH radicals.

432 A multiple regression model (MRM) was established to further quantitatively assess the

433 contribution of RH and SAT to summer O_3 concentrations in NW. The MRM has been applied in

434 a number of investigations to quantify meteorological effects on ozone evolution in China (Li et

435 al., 2019, 2020, 2021; Yan et al., 2024). For SAT and RH, the MRM model can be defined as

436 $$\ln(O_3) = \alpha + \beta_1 \ln(SAT) + \beta_2 \ln(RH) + \varepsilon, \tag{3}$$

437 where α, β_1, and β_2 are model coefficients, and ε is a random error, respectively. In the first instance,

438 we considered three provinces with significant wetting trends: Xinjiang, Gansu, and Qinghai. We

439 combined annual summer O_3, RH, and SAT from three provinces into one time series of each

440 dependent and independent variable from 1998 to 2017, yielding 60 samples for each variable.

441 Tables S4-S6 present regression coefficients and statistics of the MRM. To examine the

442 multicollinearity in the MRM, we estimated the variance inflation factor (VIF, Table S4-S6). The

443 VIFs for RH and SAT are far less than 10, indicating no multicollinearity in the model. The

444 contribution of RH and SAT to O_3 is calculated by:

445 $$\text{Contribution}_i = \frac{\left|\beta_i \times \frac{STD_i}{STD_\alpha}\right|}{\text{SUM}}, \tag{4}$$

446 where $\text{SUM} = \sum_i |\beta_i \times STD_i / STD_\alpha|$, and β_i denotes the regression coefficient of independent

447 variable i (namely, RH and SAT), STD_i is the standard deviation of regression coefficient of

448 independent variable i, and STD_α represents the standard deviation of coefficient of intercept.

449 The MRM analysis reveals that RH contributes 77.5%, 59.4%, and 46.2% to O_3 variations in

450 Xinjiang, Qinghai, and Gansu. Accordingly, SAT contributes 22.5%, 40.6%, and 53.8% to O_3

451 fluctuations in these three provinces from 1998 to 2017. The results indicate that RH has become

452 a major contributor to long-term change in O_3 concentrations, overwhelming or equivalent to

453 SAT's contributions to the O_3 trend for the past two decades, likely via interactions among

454 increasing precipitation washout and OH radical, O_3 concentration, and water vapor.

455   We further assess the contributions of precipitation, RH, SAT, winds, and PBLH (planetary

456   boundary-layer height) to O_3 evolution in NW using an extended MRM model. The results confirm

457   that RH and SAT made the most significant contributions to long-term ozone trends than other

458   meteorological variables under the long-term perspective. As seen from Fig. 5, the contribution of

459   RH (49.5%) and SAT (47.6%) to O_3 evolution in NW was almost equivalent (Fig. 5a), but the

460   SAT (92.4%) dominated in entire mainland China (Fig. 5b). Whereas the PBLH only contributed

461   about 2% to O_3 variations because the PBLH varies on a daily and hourly basis and affects

462   insignificantly (summer) seasonal changes in O_3 concentrations.

463

464
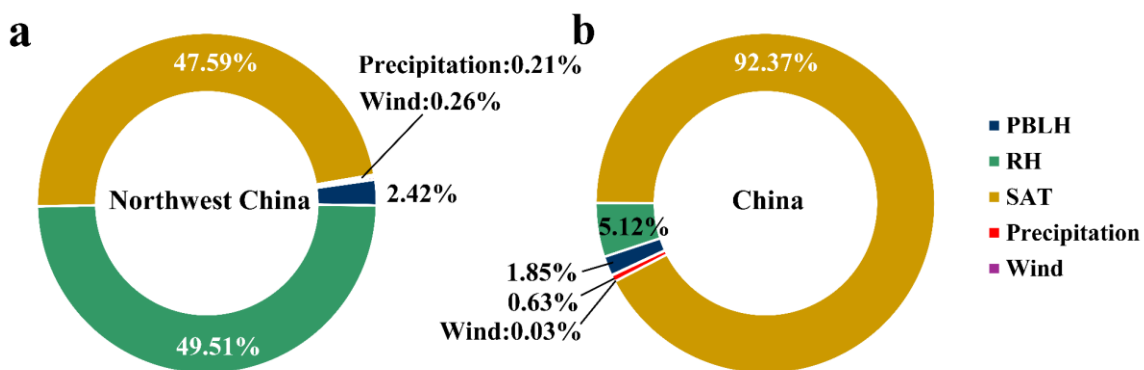
465   **Figure 5.** Contribution of PBLH (planetary boundary-layer height), RH, SAT, precipitation, and wind to O_3
466   evolution. (a) Northwest China, (b). Mainland China.

467   It should be pointed out that since the wetness also helps growing vegetation, which causes

468   increasing biogenic VOC emission (BVOC) and hence rising O_3 concentrations, the contribution

469   of BVOCs to O_3 fluctuations under increasing wetness should also be taken into consideration. To

470   examine this hypothesis, we designed an extra model scenario (S5) in which we used the updated

471   LUC data (section 2.4) and fixed LUC in 1998 in the WRF-Chem simulation and ran the model

472   from 1998 to 2017. Since the LUC defines vegetation coverage, the fixed LUC suggests no

473   vegetation change during this period. We then estimated the fractions between modeled O_3

474   concentration with fixed LUC and the baseline scenario S1 with annually-varying LUC, thereby

475   eliminating the effects from emissions, meteorology, and chemistry but highlighting the LUC (or

476   greenness) effect only. The result is illustrated in Fig. ~~S13~~S14. As shown, while the fraction

477   fluctuates positively (Xinjiang) and negatively (Northern Shaanxi and Eastern Inner Mongolia),

478   indicating increasing and decreasing O_3 levels induced by LUC or greening, the magnitudes of

479   provincial mean concentration fractions are very small, mostly ranging from -1% to 0.3%,

480   suggesting that the LUC under the wetting trend in NW plays an insignificant role in O_3 fluctuation.

3.3 Projected future climate impacts on summer Ozone

482   Given the significant impacts of wetting on O_3 evolution in NW over the past two decades,

483   concerns have also been raised regarding O_3 responses to future wetting and warming. We

484   estimated the projected O_3 concentrations, RH, and SAT fractions between the baseline and fixed

485   meteorology scenarios under the SSP2-4.5 and SSP5-8.5 pathways (section 2.6) for the years 2019,

486   2030, and 2060, respectively (Figs. 6 and 7). As mentioned earlier, since both scenarios

487   implemented the same emissions and chemistry but the baseline scenario accounted for variable

488   meteorology, the fractions (or differences) between the two scenarios eliminated the effects of

489   emissions and chemistry, thereby isolating meteorological signals only.

490
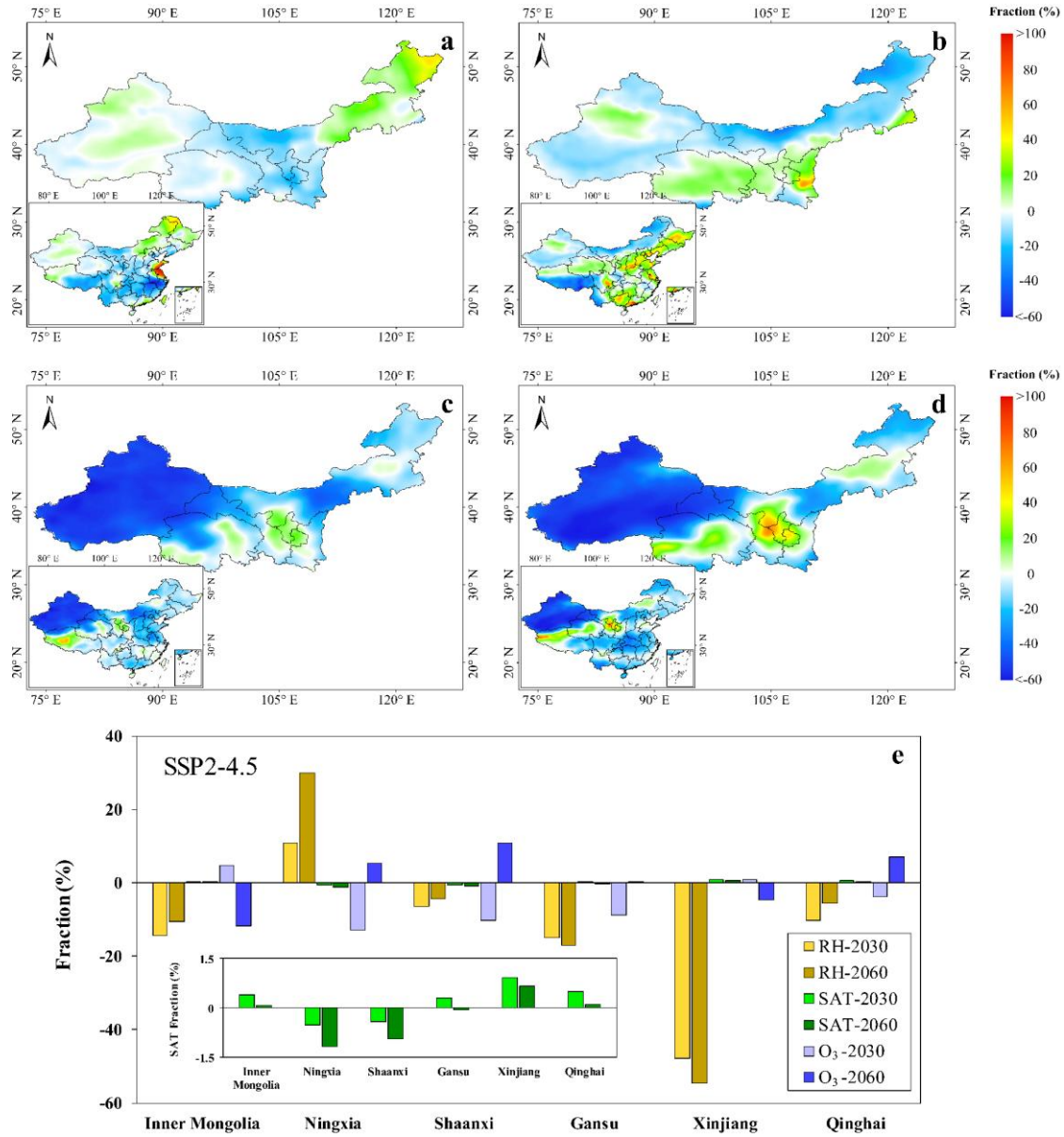
Figure 6. (a) Summer O_3 concentration fractions of 2019 to 2030 under SSP2-4.5scenario, estimated by F_{SSP245} $= (C_{2030} - C_{2019}) / C_{2019} \times 100\%$, where C_{2019} and C_{2030} are the summer surface O_3 air concentrations in 2019 and 2030, respectively, (b) same as Fig. 6a but for O_3 fractions of 2019 to 2060, (c) same as Fig. 6a but for summer RH fractions of 2019 to 2030, (d) same as Fig. 6a but for summer RH fractions of 2019 to 2060, (e) fractions of RH, SAT, and O_3 of 2019 to 2030 and 2019 to 2060 (shown in the same color bar as 2030 but with oblique lines*) in the six provinces of Northwestern China under the SSP2-4.5 scenario.

497
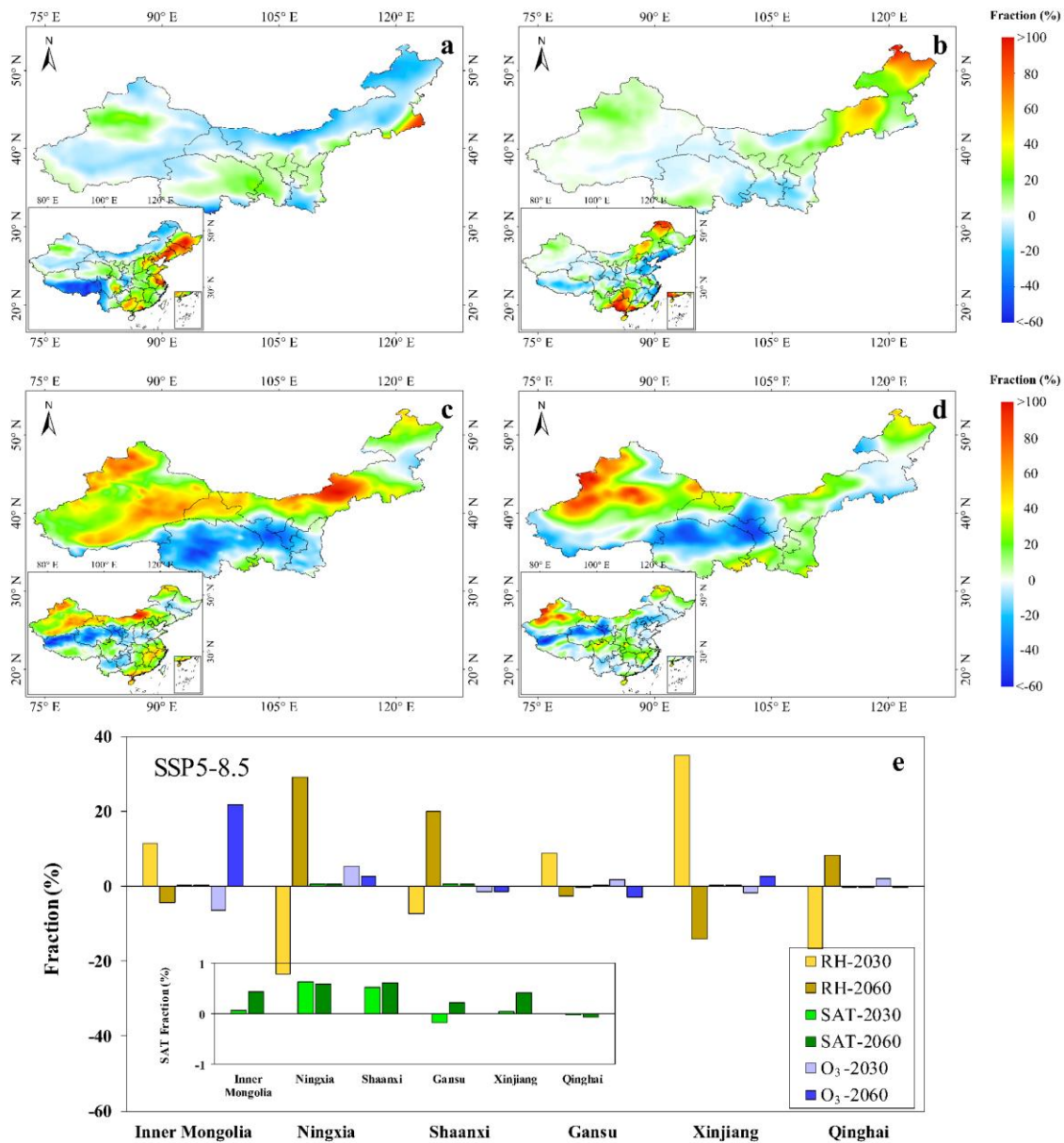
Figure 7. (a) Summer O_3 concentration fraction of 2019 to 2030 under the SSP5-8.5 scenario, estimated by $F_{SSP585} = (C_{2030} - C_{2019}) / C_{2019} \times 100\%$, where C_{2019} and C_{2030} are the summer surface O_3 air concentrations in 2019 and 2030, respectively, (b) same as Fig. 7a but for O_3 fraction of 2019 to 2060, (c) same as Fig. 7a but for summer RH fraction of 2019 to 2030, (d) same as Fig. 7a but for summer RH fraction of 2019 to 2060, (e) fractions of RH, SAT, and O_3 of 2019 to 2030 and 2019 to 2060 (shown in the same color bar as 2030 but with oblique lines) in the six provinces of Northwestern China under the SSP5-8.5 scenario.

Detailed discussions on the associations between projected O_3 evolution and trends of RH and SAT under the SSP2-4.5 and SSP5-8.5 pathways from 2019 to 2030 and from 2019 to 2060 are presented in Section S4 in the Supplement and Figs. 6-7 and Fig. ~~S14~~S15, respectively. Overall,

507   from 2019 to 2030, we observe a stronger negative association between O_3 and RH under SSP5-
508   8.5 than under SSP2-4.5 across NW, suggesting that climate conditions under the SSP5-8.5
509   scenario will more effectively suppress O_3 growth compared to SSP2-4.5 during this period.
510   However, from 2019 to 2060, the SSP5-8.5 tends to project higher O_3 levels than SSP2-4.5. From
511   a wetting trend perspective, we must determine which pathway would project a more realistic
512   future humidity trend in NW. China has been making significant strides in transitioning to
513   renewable energy sources, reducing its carbon footprint, and committing to achieve a carbon peak
514   before 2030 and carbon neutrality by 2060. These commitments align more closely with the
515   mitigation efforts outlined in SSP2-4.5, which, as manual interventions, will overshadow the
516   impact of climate change on O_3 fluctuations. There have also been debates regarding ongoing
517   wetting trends in NW based on CMIP6 projections under SSP5-8.5 and historical data analysis
518   (Huang et al., 2017). Historically, China's rapid economic growth has heavily depended on fossil
519   fuels, which may render SSP5-8.5 more applicable in China. The responses of O_3 evolution to RH
520   under SSP5-8.5 are more akin to those observed from 1998 to 2017 (section 3.2) than to SSP2-4.5.
521   In light of this, while China may achieve its carbon peak and neutrality goals, the wetting trend in
522   NW will likely persist in the coming decades, exacerbating continuous O_3 pollution in NW, in
523   addition to manual interventions. Under SSP5-8.5, the projected increase in humidity (e.g., 34.9%
524   in Xinjiang by 2030) may enhance O_3 wet deposition, partially offsetting the warming-driven O_3
525   rise. This aligns with Li et al. (2014), who identified humidity as a critical factor modulating cross-
526   regional ozone transport efficiency.
527

4. Conclusions

529   This study conducted extensive sensitivity model simulations to explore the surface O_3
530   responses to past and future climate change in Northwestern China. The results demonstrated that
531   significant wetting since the 21st century in this region, particularly in the three westernmost
532   provinces (Xinjiang, Qinghai, and Gansu) of NW, has slowed O_3 growth. We show that in these
533   provinces, the wetting influence on O_3 evolution has outweighed the warming effect and played
534   an almost equal role to warming across the entire NW. Both factors contributed approximately 50%
535   to summer O_3 variations from 1998 to 2017, among the major meteorological factors causing
536   changes in O_3 concentrations. This finding contrasts with the dominant role of warming in the

meteorological effects on O$_3$ evolution in China. We linked the increasing OH radicals, which interact with water vapor, to the declining O$_3$ trend. Given that humidification in NW is projected to continue in the coming years and that the mitigation of O$_3$ precursor emissions in China will still be implemented under the nation's air pollution control strategies, the impact of humidification on O$_3$ trends in NW will likely become more significant. Such an impact should be considered in future policymaking for the reduction of O$_3$ pollution in NW. –While this study advances our understanding of ozone-climate interactions in Northwestern China, several uncertainties warrant attentions. First, the reliance on static emission inventories (e.g., EDGAR) may underestimate dynamic sources such as soil NO$_x$ emissions, which are critical in arid region. Second, the 20 km resolution of WRF-Chem may inadequately resolve fine-scale topographic effects on local meteorology (e.g., valley breezes in mountainous Northwestern China), potentially biasing ozone simulations. Future work should integrate high-resolution emission inventories to improve accuracy. Additionally, ground-based ozone measurements in remote Northwestern China remain sparse, limiting robust model validation. Expanding monitoring networks will be essential to constrain uncertainties.

Data availability

ERA-Interim reanalysis data can be accessed at https://www.ecmwf.int/en/forecasts/datasets/reanalysisdatasets/era-interim. EDGAR dataset is available at https://edgar.jrc.ec.europa.eu/. LUC data can be accessed at http://www.resdc.cn. DPEC Inventory is available at http://meicmodel.org.cn. The meteorological data under the CMIP6 framework is collected from https://aims2.llnl.gov/search/cmip6/.

Author contributions

XZ and YY contribute equally to this article. All authors contributed to the manuscript and have given approval of the final version. XZ and HG coordinated and supervised the project. XZ, YY, WW and JM designed the present experiment, carried out modeling, and drafted the manuscript. NZ, HS, XJ, CW, and HM collected the data. XZ, YY, ZY and TH analyzed simulation results.

Competing interests

The authors declare that they have no known competing financial interests or personal relationships that could have appeared to influence the work reported in this paper.

Acknowledgements

We wish to thank the High-performance Computing Platform of Peking University to support extensive model simulations of this study.

Financial support

This research was supported by the National Natural Science Foundation of China via grants 42407134, 42177351 and 41977357.

References

Bei, N. F., Zhao, L. N., Wu, J. R., Li, X., Feng, T., and Li, G. H.: Impacts of sea-land and mountain-valley circulations on the air pollution in Beijing-Tianjin-Hebei (BTH): A case study, Environ. Pollut., 234, 429–438, https://doi.org/10.1016/j.envpol.2017.11.066, 2018.

Belan, B. D., and Savkin, D. E.: The Role of Air Humidity in Variations in Near-Surface Ozone Concentration, Atmospheric and Oceanic Optics, 32, 586–589, https://doi.org/10.1134/S1024856019050038, 2019.

Bossioli, E., Tombrou, M., Kalogiros, J., Allan, J., Bacak, A., Bezantakos, S., Biskos, G., Coe, H., Jones, B. T., Kouvarakis, G., Mihalopoulos, N., and Percival, C. J.: Atmospheric composition in the Eastern Mediterranean: Influence of biomass burning during summertime using the WRF-Chem model, Atmos Environ., 132, 317–331, https://doi.org/10.1016/j.atmosenv.2016.03.011, 2016.

Cheng, J., Tong, D., Zhang, Q., Liu, Y., Lei, Y., Yan, G., Yan, L., Yu, S., Cui, R. Y., Clarke, L., Geng, G. N., Zheng, B., Zhang, X. Y., Davis, S. J., and He, K. B.: Pathways of China's $PM_{2.5}$ air quality 2015-2060 in the context of carbon neutrality, Natl. Sci. Rev., 8, nwab078, https://doi.org/10.1093/nsr/nwab078, 2021.

Cheng, J., Tong, D., Liu, Y., Geng, G. N., Davis, S. J., He, K. B., and Zhang, Q.: A synergistic approach to air pollution control and carbon neutrality in China can avoid millions of premature deaths annually by 2060, One Earth, 6, 978–989, https://doi.org/10.1016/j.oneear.2023.07.007, 2023.

Crippa, M., Guizzardi, D., Muntean, M., Schaaf, E., Dentener, F., van Aardenne, J. A., Monni, S., Doering, U., Olivier, J. G. J., Pagliari, V., and Janssens-Maenhout, G.: Gridded emissions of air pollutants for the period 1970-2012 within EDGAR v4.3.2, Earth Syst. Sci. Data, 10, 1987–2013, https://doi.org/10.5194/essd-10-1987-2018, 2018.

Cooper, O., Parrish, D., Ziemke, J., Balashov, N., Cupeiro, M., Galbally, I., Gilge, S., Horowitz, L., Jensen, N., Lamarque, J., Naik, V., Oltmans, S., Schwab, J., Shindell, D., Thompson, A., Thouret, V., Wang, Y., and Zbinden, R.: Global distribution and trends of tropospheric ozone: An observation-based review, Elementa: Science of the Anthropocene, 2, 000029, https://doi.org/10.12952/journal.elementa.000029, 2014.

Ding, J., Dai, Q., Zhang, Y., Xu, J., Huangfu, Y., and Feng, Y.: Air humidity affects secondary aerosol formation in different pathways, Sci. Total Environ., 759, 143540, https://doi.org/10.1016/j.scitotenv.2020.143540, 2021.

Ding, J., Dai, Q., Fan, W., Lu, M., Zhang, Y., Han, S., and Feng, Y.: Impacts of meteorology and precursor emission change on O_3 variation in Tianjin, China from 2015 to 2021, J. Environ. Sci., 126, 506–516, https://doi.org/10.1016/j.jes.2022.03.010, 2023.

Ding, S., Jiang, X., and Wu, C.: Contrasting ~~Near-Surface Ozone Pollution~~near-surface ozone pollution in ~~Wet~~wet and ~~Dry Year~~dry year over China, Int. J. Environ. Res. Public Health, 20, 998, https://doi.org/10.3390/ijerph20020998, 2023.

Eck, T. F., Holben, B. N., Kim, J., Beyersdorf, A. J., Choi, M., Lee, S., Koo, J. H., Giles, D. M., Schafer, J. S., Sinyuk, A., Peterson, D. A., Reid, J. S., Arola, A., Slutsker, I., Smirnov, A., Sorokin, M., Kraft, J., Crawford, J. H., Anderson, B. E., Thornhill, K. L., Diskin, G., Kim, S. W., and Park, S.: Influence of cloud, fog, and

615   high relative humidity during pollution transport events in South Korea: Aerosol properties and PM$_{2.5}$
616   variability, Atmos. Environ., 232, 117530, https://doi.org/10.1016/j.atmosenv.2020.117530, 2020.

617 Emmons, L. K., Walters, S., Hess, P. G., Lamarque, J. F., Pfister, G. G., Fillmore, D., Granier, C., Guenther, A.,
618   Kinnison, D., Laepple, T., Orlando, J., Tie, X., Tyndall, G., Wiedinmyer, C., Baughcum, S. L., Kloster, S.:
619   Description and evaluation of the model for ozone and related chemical tracers, version 4 (MOZART-4),
620   Geosci. Model. Dev., 3, 43–67, https://doi.org/10.5194/gmd-3-43-2010, 2010.

621 Eyring, V., Bony, S., Meehl, G. A., Senior, C. A., Stevens, B., Stouffer, R. J., and Taylor, K. E.: Overview of
622   the Coupled Model Intercomparison Project Phase 6 (CMIP6) experimental design and organization,
623   Geosci. Model Dev., 9, 1937–1958, https://doi.org/10.5194/gmd-9-1937-2016, 2016.

624 Ghazali, S., Awang, N. R., Karim, M. F. A., and Muhammad, M.: Fluctuational Analysis of Nighttime Ground-
625   Level Ozone Concentrations due to Variations in Hourly Relative Humidity, Smart Environmental Science,
626   Technology and Management, 1, 118–121, https://doi.org/10.36647/978-93-92106-02-6.21, 2022.

627 Gong, C., Yue, X., Liao, H., and Ma, Y. M.: A humidity-based exposure index representing ozone damage
628   effects on vegetation, Environ. Res. Lett., 16, 044030, https://doi.org/10.1088/1748-9326/abecbb, 2021.

629 Guenther, A., Karl, T., Harley, P., Wiedinmyer, C., Palmer, P. I., and Geron, C.: Estimates of global terrestrial
630   isoprene emissions using MEGAN (Model of Emissions of Gases and Aerosols from Nature), Atmos. Chem.
631   Phys., 6, 3181–3210, https://doi.org/10.5194/acp-6-3181-2006, 2006.

632 Guenther, A. B., Jiang, X., Heald, C. L., Sakulyanontvittaya, T., Duhl, T., Emmons, L. K., and Wang, X.: The
633   Model of Emissions of Gases and Aerosols from Nature version 2.1 (MEGAN2.1): an extended and updated
634   framework for modeling biogenic emissions, Geosci. Model Dev., 5, 1471–1492,
635   https://doi.org/10.5194/gmd-5-1471-2012, 2012.

636 Han, S., Bian, H., Feng, Y., Liu, A., Li, X., Zeng, F., and Zhang, X.: Analysis of the Relationship between O$_3$,
637   NO and NO$_2$ in Tianjin, China, Aerosol Air Qual. Res., 11, 128–139,
638   https://doi.org/10.4209/aaqr.2010.07.0055, 2011.

639 Huang, J. P., Yu, H. P., Dai, A. G., Wei, Y., and Kang, L. T.: Drylands face potential threat under 2 °C global
640   warming target, Nat. Clim. Chang., 7, 417–422, https://doi.org/10.1038/nclimate3275, 2017.

641 Hu, F., Xie, P., Xu, J., Lv, Y., Zhang, Z., Zheng, J., and Tian, X.: Long-term trends of ozone in the Yangtze
642   River Delta, China: Spatiotemporal impacts of meteorological factors, local, and non-local emissions, J.
643   Environ. Sci., 7,10–33, https://doi.org/10.1016/j.jes.2024.07.017, 2024.

644 Kendall, M. G.: Rank Correlation Methods, Mathematics, https://doi.org/10.2307/1402637, 1949.

645 Kerr, G. H., Waugh, D. W., Steenrod, S. D., Strode, S. A., and Strahan, S. E.: Surface Ozone-Meteorology
646   Relationships: Spatial Variations and the Role of the Jet Stream, J. Geophys. Res-Atmos., 125,
647   e2020JD032735, https://doi.org/10.1029/2020JD032735, 2020.

648 El-Shaarawi, A. H., and Niculescu, S. P.: On kendall's tau as a test of trend in time series data, Environmetrics,
649   3, 385–411, https://doi.org/10.1002/env.3170030403, 1992.

650 Koster, R. D., Dirmeyer, P. A., Guo, Z. C., Bonan, G., Chan, E., Cox, P., Gordon, C. T., Kanae, S., Kowalczyk,
651   E., Lawrence, D., Liu, P., Lu, C. H., Malyshev, S., McAvaney, B., Mitchell, K., Mocko, D., Oki, T., Oleson,
652   K., Pitman, A., Sud, Y. C., Taylor, C. M., Verseghy, D., Vasic, R., Xue, Y. K., Yamada, T., and Team, G.:
653   Regions of strong coupling between soil moisture and precipitation, Science, 305, 1138–1140,
654   https://doi.org/10.1126/science.1100217, 2004.

655 Kleeman, M. J.: A preliminary assessment of the sensitivity of air quality in California to global change, Climatic
656   Change, 87, 273–292, https://doi.org/10.1007/s10584-007-9351-3, 2008.

657 Li, B., Chen, Y., and Shi, X.: Why does the temperature rise faster in the arid region of northwest China? J.
658   Geophys. Res-Atmos., 117, D16115, https://doi.org/10.1029/2012JD017953, 2012.

659 Li, J., Yang, W., Wang, Z., Chen, H., Hu, B., Li, J., Sun, Y., Fu, P., Zhang, Y.: Modeling study of surface ozone
660   source   receptor   relationships   in   East   Asia,   Atmos.   Res.   167,   77–88,
661   https://doi.org/10.1016/j.atmosres.2015.07.010, 2016.

662 Li, J. X., Wang, Z. X., Chen, L. L., Lian, L. L., Li, Y., Zhao, L. Y., Zhou, S., Mao, X. X., Huang, T., Gao, H.,
663   and Ma, J. M.: WRF-Chem simulations of ozone pollution and control strategy in petrochemical
664   industrialized and heavily polluted Lanzhou City, NW, Sci. Total Environ., 737, 139835,
665   https://doi.org/10.1016/j.scitotenv.2020.139835, 2020.

666 Li, K., Jacob, D. J., Liao, H., Shen, L., Zhang, Q., and Bates, K. H.: Anthropogenic drivers of 2013-2017 trends
667   in   summer   surface   ozone   in   China,   Proc.   Natl.   Acad.   Sci.   U.S.A.,   116,   422–427,
668   https://doi.org/10.1073/pnas.1812168116, 2019.

669 Li, K., Jacob, D. J., Liao, H., Qiu, Y. L., Shen, L., Zhai, S. X., Bates, K. H., Sulprizio, M. P., Song, S. J., Lu, X.,
670   Zhang, Q., Zheng, B., Zhang, Y. L., Zhang, J. Q., Lee, H. C., and Kuk, S. K.: Ozone pollution in the North
671   China Plain spreading into the late-winter haze season, Proc. Natl. Acad. Sci. U.S.A., 118, e2015797118,
672   https://doi.org/10.1073/pnas.2015797118, 2021.

673 Li, K., Jacob, D. J., Shen, L., Lu, X., De Smedt, I., and Liao, H.: Increases in surface ozone pollution in China
674   from 2013 to 2019: anthropogenic and meteorological influences, Atmos. Chem. Phys., 20, 11423–11433,
675   https://doi.org/10.5194/acp-20-11423-2020, 2020.

676 Li, L., Liu, N., Shen, L., Zhao, Z., Wang, H., Wang, Y., Li, X., and Ma, Y.: Ozone concentration at various
677   heights near the surface layer in Shenyang, Northeast China, Front. Environ. Sci., 10, 1011508,
678   https://doi.org/10.3389/fenvs.2022.1011508, 2022.

679 Li, M., Yu, S., Chen, X., Li, Z., Zhang, Y., Wang, L., Liu, W., Li, P., Lichtfouse, E., Rosenfeld, D., and Seinfeld,
680   J. H.: Large scale control of surface ozone by relative humidity observed during warm seasons in China,
681   Environ. Chem. Lett., 19, 3981–3989, https://doi.org/10.1007/s10311-021-01265-0, 2021.

682 Li, X., Liu, J., Mauzerall, D. L., Emmons, L. K., Walters, S., Horowitz, L. W., Tao, S.: Effects of trans-Eurasian
683   transport of air pollutants on surface ozone concentrations over Western China, J. Geophys. Res. Atmos.,
684   119, 12338–12354, https://doi.org/10.1002/2014JD021936, 2014.

685 Li, X. B., Yuan, B., Parrish, D. D., Chen, D. H., Song, Y. X., Yang, S. X., Liu, Z. J., and Shao, M.: Long-term
686   trend of ozone in southern China reveals future mitigation strategy for air pollution, Atmos. Environ., 269,
687   118869, https://doi.org/10.1016/j.atmosenv.2021.118869, 2022.

688 Lian, X., Piao, S. L., Chen, A. P., Huntingford, C., Fu, B. J., Li, L., Huang, J. P., Sheffield, J., Berg, A. M.,
689   Keenan, T. F., McVicar, T. R., Wada, Y., Wang, X. H., Wang, T., Yang, Y. T., and Roderick, M. L.:
690   Multifaceted characteristics of dryland aridity changes in a warming world, Nat. Rev. Earth Env., 2, 232–
691   250, https://doi.org/10.1038/s43017-021-00144-0, 2021.

692 Liao, J. B., Wang, T. J., Jiang, Z. Q., Zhuang, B. L., Xie, M., Yin, C. Q., Wang, X. M., Zhu, J. L., Fu, Y., and
693   Zhang, Y.: WRF/Chem modeling of the impacts of urban expansion on regional climate and air pollutants
694   in   Yangtze   River   Delta,   China,   Atmos.   Environ.,   106,   204–214,
695   https://doi.org/10.1016/j.atmosenv.2015.01.059, 2015.

696 Liu, X., Zhang, D., Luo, Y., and Liu, C.: Spatial and temporal changes in aridity index in northwest China: 1960
697   to 2010, Theor. Appl. Climatol., 112, 307–316, https://doi.org/10.1007/s00704-012-0734-7, 2013.

698 Lu, X., Ye, X. P., Zhou, M., Zhao, Y. H., Weng, H. J., Kong, H., Li, K., Gao, M., Zheng, B., Lin, J. T., Zhou,
699   F., Zhang, Q., Wu, D. M., Zhang, L., and Zhang, Y. H.: The underappreciated role of agricultural soil
700   nitrogen oxide emissions in ozone pollution regulation in North China, Nat. Commun., 12, 5021,
701   https://doi.org/10.1038/s41467-021-25147-9, 2021.

702 Ma, S., Shao, M., Zhang, Y., Dai, Q., and Xie, M.: Sensitivity of $PM_{2.5}$ and O_3 pollution episodes to
703   meteorological   factors   over   the   North   China   Plain,   Sci.   Total.   Environ.,   792,   148474,
704   https://doi.org/10.1016/j.scitotenv.2021.148474, 2021.

Madden, R. A., and Williams, J.: The Correlation between Temperature and Precipitation in the United States and Europe, Mon. Weather Rev., 106, 142–147, https://doi.org/10.1175/1520-0493(1978)106<0142:TCBTAP>2.0.CO;2, 1978.

Mann, H. B.: Nonparametric Tests Against Trend, Econometrica, 13, 245, https://doi.org/10.2307/1907187, 1945.

Millstein, D. E., and Harley, R. A.: Impact of climate change on photochemical air pollution in Southern California, Atmos. Chem. Phys., 9, 3745–3754, https://doi.org/10.5194/acp-9-3745-2009, 2009.

Mo, J. Y., Huang, T., Zhang, X. D., Zhao, Y., Liu, X., Li, J. X., Gao, H., and Ma, J. M.: Spatiotemporal distribution of nitrogen dioxide within and around a large-scale wind farm - a numerical case study, Atmos. Chem. Phys., 17, 14239–14252, https://doi.org/10.5194/acp-17-14239-2017, 2017.

Nie, J. S., Wang, W. H., Heermance, R., Gao, P., Xing, L., Zhang, X. J., Zhang, R., Garzione, C., and Xiao, W. J.: Late Miocene Tarim desert wetting linked with eccentricity minimum and East Asian monsoon weakening, Nat. Commun., 13, 3977, https://doi.org/10.1038/s41467-022-31577-w, 2022.

Peng, D., and Zhou, T.: Why was the arid and semiarid northwest China getting wetter in the recent decades? J. Geophys. Res-Atmos., 122, 9060–9075, https://doi.org/10.1002/2016JD026424, 2017.

Pfannerstill, E. Y., Arata, C., Zhu, Q., Schulze, B. C., Ward, R., Woods, R., Harkins, C., Schwantes, R. H., Seinfeld, J. H., Bucholtz, A., Cohen, R. C., and Goldstein, A. H.: Temperature-dependent emissions dominate aerosol and ozone formation in Los Angeles, Science, 384, 1324–1329, https://doi.org/10.1126/science.adg8204, 2024.

Shi, P. Y., Tilgner, M., and Lo, M. K.: Construction and characterization of subgenomic replicons of New York strain of West Nile virus, Virology, 296, 219–233, https://doi.org/10.1006/viro.2002.1453, 2002.

Tie, X., Madronich, S., Li, G., Ying, Z., Weinheimer, A., Apel, E., and Campos, T.: Simulation of Mexico City plumes during the MIRAGE-Mex field campaign using the WRF-Chem model, Atmos Chem. Phys., 9, 4621–4638, https://doi.org/10.5194/acp-9-4621-2009, 2009.

Tong, D., Cheng, J., Liu, Y., Yu, S., Yan, L., Hong, C. P., Qin, Y., Zhao, H. Y., Zheng, Y. X., Geng, G. N., Li, M., Liu, F., Zhang, Y. X., Zheng, B., Clarke, L., and Zhang, Q.: Dynamic projection of anthropogenic emissions in China: methodology and 2015-2050 emission pathways under a range of socio-economic, climate policy, and pollution control scenarios, Atmos. Chem. Phys., 20 (9), 5729–5757, https://doi.org/10.5194/acp-20-5729-2020, 2020.

Wang, J., Li, J., Li, X., Wang, D., and Fang, C.: Relationship between ozone and air temperature in future conditions: A case study in Sichuan basin, China, Environ. Pollut., 343, 123276, https://doi.org/10.1016/j.envpol.2023.123276, 2024.

Wang, Z. B., Li, J. X., and Liang, L. W.: Spatio-temporal evolution of ozone pollution and its influencing factors in the Beijing-Tianjin-Hebei Urban Agglomeration, Environ. Pollut., 256, 113419, https://doi.org/10.1016/j.envpol.2019.113419, 2020.

Wild, O., Zhu, X., and Prather, M. J.: Fast-J: Accurate Simulation of In- and Below-Cloud Photolysis in Surface Chemical Models, J. Atmos. Chem., 37, 245–282, https://doi.org/10.1023/A:1006415919030, 2000.

Yan, D., Jin, Z. P., Zhou, Y. T., Li, M. M., Zhang, Z. H., Wang, T. J., Zhuang, B. L., Li, S., and Xie, M.: Anthropogenically and meteorologically modulated summertime ozone trends and their health implications since China's clean air actions, Environ. Pollut., 343, 123234, https://doi.org/10.1016/j.envpol.2023.123234, 2024.

Yang, P., Xia, J., Zhang, Y. Y., and Hong, S.: Temporal and spatial variations of precipitation in Northwest China during 1960-2013, Atmos. Res., 183, 283–295, https://doi.org/10.1016/j.atmosres.2016.09.014, 2017.

Yang, X. Y., Li, D. W., Yang, Z., Wu, K., Ji, L. Y., Zhou, Z. Q., and Lu, Y. Q.: Revealing historical observations and future projections of precipitation over Northwest China based on dynamic downscaled CMIP6 simulations, Front. Earth Sci., 10, 1090221, https://doi.org/10.3389/feart.2022.1090221, 2023.

751 Yao, J. Q., Mao, W. Y., Chen, J., and Dilinuer, T.: Recent signal and impact of wet-to-dry climatic shift in
752   Xinjiang, China, J. Geog. Sci., 31, 1283–1298, https://doi.org/10.1007/s11442-021-1898-9, 2021.

753 Yu, R. X., Liu, M. X., Li, L., Song, J. Y., Sun, R. D., Zhang, G. J., Xu, L., and Mu R. L.: Spatial and Temporal
754   Variation of Atmospheric Ozone Column Concentration and Influencing Factors in the Yangtze River Delta
755   Region in Recent 15 Years, Acta Scientiae Circumstantiae, 41, 770–784,
756   https://doi.org/10.13671/j.hjkxxb.2020.0346, 2021.

757 Zhang, X. D., Du, J., Zhang, L. M., Huang, T., Gao, H., Mao, X. X., and Ma, J. M.: Impact of afforestation on
758   surface ozone in the North China Plain during the three-decade period, Agric. For. Meteorol., 287,
759   https://doi.org/10.1016/j.agrformet.2020.107979, 107979, 2020.

760 Zhang, X. D., Jian, X. H., Zhao, Y., Liu, X. R., Chen, K. J., Wang, L. F., Tao, S., Liu, J. F., Huang, T., Gao, H.,
761   Liu, Y. J., Zhugu, R. R., and Ma, J. M.: Tropospheric Ozone Perturbations Induced by Urban Land
762   Expansion in China from 1980 to 2017, Environ. Sci. Technol., 56, 6978–6987,
763   https://doi.org/10.1021/acs.est.1c06664, 2022.

764 Zhang, X. D., Zhugu, R. Y., Jian, X., Liu, X., Chen, K., Tao, S., Liu, J., Gao, H., Huang, T., and Ma, J. M.:
765   Associations of interannual variation in summer surface ozone with the Western Pacific Subtropical High
766   in China from 1999 to 2017, Atmos. Chem. Phys., 23, 15629–15642, https://doi.org/10.5194/acp-23-15629-
767   2023, 2023.